

## ARTICLE



# Epiblast fragmentation by shedding—a novel mechanism to eliminate cells in post-implantation mouse embryos

Rivi Halimi<sup>1</sup>, Smadar Levin-Zaidman<sup>2</sup>, Vered Levin-Salomon<sup>1</sup>, Shani Bialik<sup>1</sup> and Adi Kimchi<sup>1</sup> <sup>✉</sup>

© The Author(s), under exclusive licence to ADMC Associazione Differenziamento e Morte Cellulare 2021

The role of programmed cell death during embryonic development has been described previously, but its specific contribution to peri- and post-implantation stages is still debatable. Here, we used transmission electron microscopy and immunostaining of E5.5–7.5 mouse embryos to investigate death processes during these stages of development. We report that in addition to canonical apoptosis observed in E5.5–E7.5 embryos, a novel type of cell elimination occurs in E7.5 embryos among the epiblasts at the apical side, in which cells shed membrane-enclosed fragments of cytosol and organelles into the lumen, leaving behind small, enucleated cell remnants at the apical surface. This process is caspase-independent as it occurred in Apaf1 knockout embryos. We suggest that this novel mechanism controls epiblast cell numbers. Altogether, this work documents the activation of two distinct programs driving irreversible terminal states of epiblast cells in the post-implantation mouse embryo.

*Cell Death & Differentiation* (2022) 29:1255–1266; <https://doi.org/10.1038/s41418-021-00918-5>

## INTRODUCTION

The critical role of apoptosis during embryonic development has been widely studied [1], specifically post-gastrulation when it functions to balance cell proliferation and limit cell number, sculpt specific organs during organogenesis and morphogenesis [2–4], and eliminate excess and abnormal neuronal connections during vertebrate nervous system development [5]. In mammals, in contrast to lower organisms, apoptosis also occurs during early embryogenesis, prior to gastrulation [6]. In the blastocyst, apoptosis is prevalent among the inner cell mass, eliminating cells that fail to translocate to the correct position for their subsequent fate [6–9]. The participation of apoptosis during the late peri- and early post-implantation stages of embryonic development is less clear, however, specifically during early egg cylinder formation when the pro-amniotic cavity is formed. At this stage, the embryo acquires a cup-like shape made of two cell layers, the inner epiblast layer that surrounds the lumen, and the outer visceral endoderm. Studies in mouse embryoid bodies, 3D structures generated from pluripotent embryonic stem cells that model embryonic development, suggested that the cavity is formed by selective death of the central solid mass of epiblast cells [10–12]. This hypothesis, however, was challenged by a seminal paper conducted on mouse embryos, which suggested that formation of the central lumen results from polarization cues derived from the surrounding basement membrane (BM) that lead to the rearrangement of epiblast cells into a rosette-like structure, and actomyosin dependent apical constriction that forces the opening of a cavity [13]. A combination of loss of adhesion factors (e.g., E-cadherin) from the apical membrane and recruitment of anti-adhesion molecules, together with fluid influx generated by cellular ion pumps and released by dividing cells, contributes to

the formation and expansion of the lumen [14]. Altogether, this model called into question the relevance of apoptosis for cavitation in the peri-implantation embryo. Yet, epiblasts cells are apoptosis-competent at this stage, as observed in  $\beta$ 1-integrin deleted mouse embryos, and in drug-manipulated mosaic embryos as a means to remove aneuploid cells [15, 16]. Analogously, apoptosis may develop concomitantly with the polarization process during the peri-implantation stage, for example, to remove damaged cells or those that fail to form the proper structure.

The early post-implantation stage involves significant changes in the organization and shape of the epiblast layer, which displays an extremely high mitotic index, resulting in a rapid increase in cell number and expansion of the lumen [17–21]. At E6.5, gastrulation begins at the posterior side of the mouse embryo in the primitive streak [22], forming three germ layers, the ectoderm, mesoderm, and endoderm, by the end of E7.5 [23]. It is not known whether any cell death mechanisms are activated to counter-balance the rapid proliferation and to maintain the optimal cavity shape/size during these critical post-implantation stages. Previous reports suggested that apoptosis may occur in these stages [24, 25]. Yet, the lack of an early developmental phenotype in mice deleted of essential apoptosis genes [26] suggests that apoptosis is not critical for development at peri- and post-implantation stages. Accordingly, alternative death pathways may function together with, and/or compensate for apoptosis during these stages of development. A more thorough investigation of cell death following gastrulation is necessary to address these issues.

Here, we confirm the appearance of apoptotic cells within the epiblast layer and the lumen of E5.5–E7.5 embryos. In addition,

<sup>1</sup>Department of Molecular Genetics, Weizmann Institute of Science, Rehovot 7610001, Israel. <sup>2</sup>Department of Chemical Research Support, Weizmann Institute of Science, Rehovot 7610001, Israel. <sup>✉</sup>email: [adi.kimchi@weizmann.ac.il](mailto:adi.kimchi@weizmann.ac.il)

Edited by M. Piacentini

Received: 16 August 2021 Revised: 24 November 2021 Accepted: 26 November 2021

Published online: 7 January 2022

and most importantly, we report the existence of a second type of terminal cell fate in epiblast cells at the apical side of E7.5 embryos, which consists of shedding of cytosolic content and condensed nuclei into the lumen in a caspase-independent manner. This irreversible, terminal state serves to generate small enucleated cells at the apical surface and possibly limits cell proliferation within the post-implantation embryo.

## RESULTS

### Caspase-dependent apoptosis is activated in the peri- and post-implantation embryo

To determine whether apoptosis accompanies the rapid expansion of the amniotic cavity and enhanced epiblast proliferation between E5.5 and E7.5 [19], C57BL/6J $\text{OlaHsd}$  mouse embryos were examined at different stages for apoptotic markers. Terminal deoxynucleotidyl transferase dUTP nick end labeling (TUNEL) staining, and immunostaining for active caspases of the intrinsic mitochondrial pathway, were performed in whole-mount embryos and for higher resolution, by immunohistochemistry staining of paraffin sections (IHC-P). Fragmented nuclei characteristic of apoptotic cells (Fig. 1A) and positive TUNEL staining (Fig. 1B) were observed in E5.5 embryos, mostly in the forming cavity and also among epiblast cells forming the rosette. Furthermore, active cleaved caspase-3 and caspase-9 were observed in these regions in both whole-mount embryos and IHC-P staining (Fig. 1C–F), representing a small but significant and reproducible number of cells in each embryo examined (Fig. 1E). Caspase-6 activity was also evident, as assessed by staining for cleaved lamin A, an exclusive substrate of caspase-6 [27] (Fig. 1G). E6.5 embryos likewise stained positive for active caspase-3 in the cavity and distal epiblast (Fig. S1A). Positive TUNEL staining was observed within the epiblast layer of E7.5 embryos, as previously reported [24], mostly in the distal anterior region (Fig. 2A). Active caspase-3 was also prominent within the distal anterior region of the epiblast (Fig. 2B, C). This signal co-localized with trace nuclear content that was observed only on high exposure of DAPI signal (Fig. S1B), and was found within intact cells delineated by E-cadherin staining (Fig. 2D). This was suggestive of clearance of apoptotic bodies, which was confirmed by transmission electron microscopy (TEM). Apoptotic cells containing condensed and fragmented nuclei were observed engulfed by intact neighboring epiblast cells, at different stages of cytosolic and nuclear digestion (Fig. 2E). The size of the engulfed apoptotic cells measured in TEM was similar to that of the round cleaved caspase-3 signal observed by IHC-P (Fig. 2F). Thus, cells that undergo apoptosis within the epiblast layer are engulfed by neighboring cells, reflecting a rapid mechanism of clearance of dying cells. Notably, autophagosomes were not detected in these TEM sections (Fig. 2E) and staining for lipidated LC3-II was negative, as opposed to the stained autophagosomes observed in the 8-cell embryo and blastocyst (Fig. S2), thus excluding possible involvement of autophagy or autophagic cell death in E7.5 embryos.

In addition to the engulfed apoptotic cells observed within the epiblast in E7.5 embryos, active caspase-3 was also detected in the cavity, overlapping with fragmented nuclei (Figs. 2B and 3A). Surprisingly, condensed, round non-fragmented nuclei, which were surrounded by weak phalloidin staining and were negative for cleaved caspase-3, were also present in the lumen (Fig. 3B). Round condensed nuclei surrounded by trace cytosol with weak caspase activity were also identified (Fig. 3C). The presence of these different forms of nuclei in the lumen prompted us to further investigate the morphology of the apical epiblasts in detail.

### Epiblast cells at the apical side shed their content into the lumen in E7.5 embryos

In order to identify the origin of the condensed nuclei within the lumen, E7.5 embryos were stained for the membrane-localized

E-cadherin to delineate cell borders, to facilitate a closer examination of the epiblasts layer. Several small and rounded cells with condensed, round nuclei were observed, significantly differing in shape and size (8  $\mu\text{m}$  diameter) from most of the epiblast nuclei, which were elongated with an average size of 11  $\mu\text{m} \times 20 \mu\text{m}$  ( $w \times l$ ) (Fig. 4A). These were not mitotic cells, as their nuclei did not stain for the mitosis marker phospho-histone H3 (pHH3) (Fig. 4B, C, Movie 1, Movie 2), in contrast to the mitotic epiblasts at the apical side identified by DAPI staining at different mitotic stages, which were positive for pHH3. The condensation of the pHH3-negative nuclei may precede nuclear extrusion, similar to what occurs during the process of erythrocyte enucleation [28]. Indeed, several small cells seemed to be lacking nuclei altogether (white arrows, right panels Fig. 4A). As E-cadherin is not expressed on the apical membrane, staining for Podocalyxin was performed in serial sagittal sections of the embryo to examine the apical surface and intracellular contents of these cells by immunostaining of frozen sections. This analysis revealed small cells at the apical side, abutting the cavity, which lacked detectable DAPI staining throughout the 6  $\mu\text{m}$  examined while retaining Podocalyxin and phalloidin staining (Fig. 4D). The lack of nuclei can be clearly seen in a 3D reconstruction of the images, presented from the point of view of the lumen, with phalloidin staining of F-actin at the apical cell surfaces facing the viewer (Movie 3). Interestingly, the condensed round nuclei in the small epiblasts were of similar size to the condensed nuclei observed in the lumen described above (Fig. 3B, C). The similarity suggested that the source of these free nuclei were the enucleated cells on the apical side. In support of this, staining for Podocalyxin revealed vesicles of varying size budding from the apical membrane, and apical-derived Podocalyxin-positive membranes were observed within the lumen (Fig. 4E). Similar observations were made on hematoxylin and eosin (H&E) stained sections; cell debris consisting of free nuclei or nuclei surrounded by trace cytoplasm was observed within the lumen, and small cells lacking nuclei were found at the apical surface (Fig. 4F). Eosin staining of these cells was fainter, most likely due to partial loss of cytoplasmic content. This implies that apical epiblasts shed contents to the lumen, including intact nuclei.

TEM of transverse sections of E7.5 embryos was performed to more closely examine the shedding process. Epiblast cells display a pseudostratified morphology, attached to the BM at the basal side and extending towards the apical side, with an elongated nucleus occupying most of the cell (Fig. S3Aa, b). The average size of the pseudostratified epiblast cell measured in TEM images was 9  $\times$  18  $\mu\text{m}$  (Fig. S3Aa, b). In contrast, among the epiblast cells at the apical side surrounding the lumen, small (between 2 and 5  $\mu\text{m}$ ), non-polarized cells were detected in all 8 embryos examined, which were depleted of their nuclei, without any apparent contact to the BM. Some of these small enucleated epiblasts contained mitochondria (Fig. 5Aa, b) or other cytosolic organelles (Fig. 5Ac–e, 5Ai), while in others, defined organelles could not be detected (5Ag). These were reminiscent of the small enucleated cells visualized in Fig. 4 and Movie 3. These cells shed portions of their cytoplasmic content, heterogeneous in nature, into the lumen (Fig. 5Aa–i; red arrows, Fig. S3Ac, d). These cellular fragments, surrounded by membrane, ranged in size from 100 nm to 2  $\mu\text{m}$  and contained various organelles, such as intact mitochondria, smooth and rough ER. The extruded cytosolic fragments differed in size and content from microvilli at the apical side (Fig. 5Ag–i; Fig. S3Ac, d).

In order to establish the absence of nuclei in these apical cells, focused ion beam scanning electron microscopy (FIB-SEM) volume imaging of E7.5 embryos was performed, focusing on one of the small cells in the apical region (Fig. S3B). The total analyzed volume was 9.8  $\times$  8.7  $\times$  5.8  $\mu\text{m}$ . Nuclear content was not detected in any of the 580 parallel sections, spaced 10 nm apart (Movie 4). These small, enucleated cells were scattered among the other

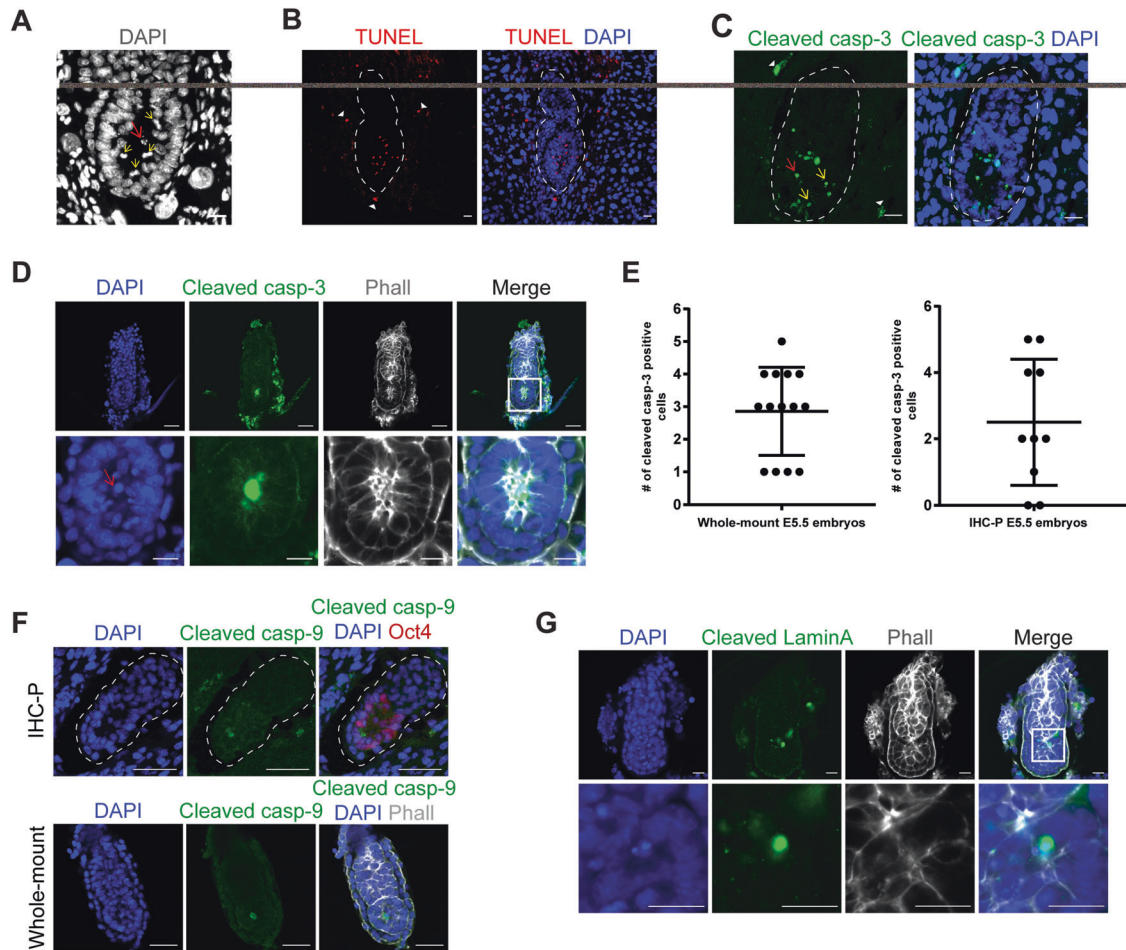


**Fig. 1 Caspase-dependent apoptosis is activated in the peri-implantation embryo at E5.5.** **A** IHC-P staining of the E5.5 embryo showing fragmented nuclei in the lumen (marked by red arrow) and mitotic cells among the epiblasts at the apical side (marked by yellow arrows). Nuclei were stained with DAPI (white). **B** IHC-P staining of E5.5 embryo for TUNEL (red). Nuclei were counterstained with DAPI (blue). White arrowhead indicates a positive TUNEL signal in the uterine tissue. The white dashed line delineates the boundaries of the embryo. Shown is a representative image from eight sections ( $n = 4$  embryos) examined. **C** IHC-P staining of E5.5 embryo for cleaved caspase-3 (green), nuclei were counterstained with DAPI (blue). The white dashed line delineates the boundaries of the embryo. Red and yellow arrows mark fragmented nuclei stained by caspase-3 in the lumen and among the epiblasts, respectively. White arrowhead indicates a positive caspase signal in the uterine tissue. Shown is a representative image taken from one of ten embryos examined. **D** Whole-mount staining of E5.5 embryo for cleaved caspase-3 (green), F-actin (phalloidin, white), and nuclei (DAPI, blue). Lower panels are higher magnification views of the boxed region in upper panels. The high signal of cleaved caspase-3 co-localizing with a fragmented nucleus in the lumen is marked by the red arrow. Shown is a representative image taken from one of 14 embryos examined, from 9 different litters stained in separate experiments. **E** Quantitation of cleaved caspase-3 positive cells, detected by whole-mount staining (left panel) or IHC-P (right panel) in E5.5 embryos. Each dot represents one embryo, the black bar is mean  $\pm$  SD ( $n = 14$  or 10 embryos, respectively). **F** Upper panel—IHC-P staining of E5.5 embryo for cleaved caspase-9 (green), Oct4 (red, marker for pluripotent epiblast), nuclei (DAPI, blue). The white dashed line delineates the embryo boundaries. Lower panel—whole-mount staining of E5.5 embryo for cleaved caspase-9 (green), F-actin (phalloidin, white), and nuclei (DAPI, blue). **G** Whole-mount staining of E5.5 embryo for cleaved Lamin A (green), F-actin (phalloidin, white), and nuclei (DAPI, blue). Lower panels are a higher magnification view of the boxed region in upper panels. Fragmented nuclei co-localizing with cleaved Lamin A are marked by the red arrow. Scale bars in all panels: 20  $\mu$ m.

epiblast cells at the apical side, the majority of which were at different phases of mitosis (Fig. S3Ab), consistent with the pHH3 staining (Fig. 4B).

Interestingly, the lumen also contained mitochondria and rough ER without surrounding membrane (Fig. 5Ba). These membrane-free organelles may be digestion products of the extruded cytoplasmic fragments. In addition, the naked nuclei described above may be the result of degradation of cytoplasm surrounding nuclei floating in the lumen (Fig. 5Ba). In some cases, the membrane-less mitochondria and ER in the lumen were swollen (Fig. 5Bb), perhaps representing a later stage of the phenomena shown in Fig. 5Ba. Notably, large homogeneous vesicles (2–7  $\mu$ m) containing one type of organelle were also detected (Fig. 5Bc, d; Fig. S3C). One such vesicle was identified as a ribo-vesicle; the vesicle contained only

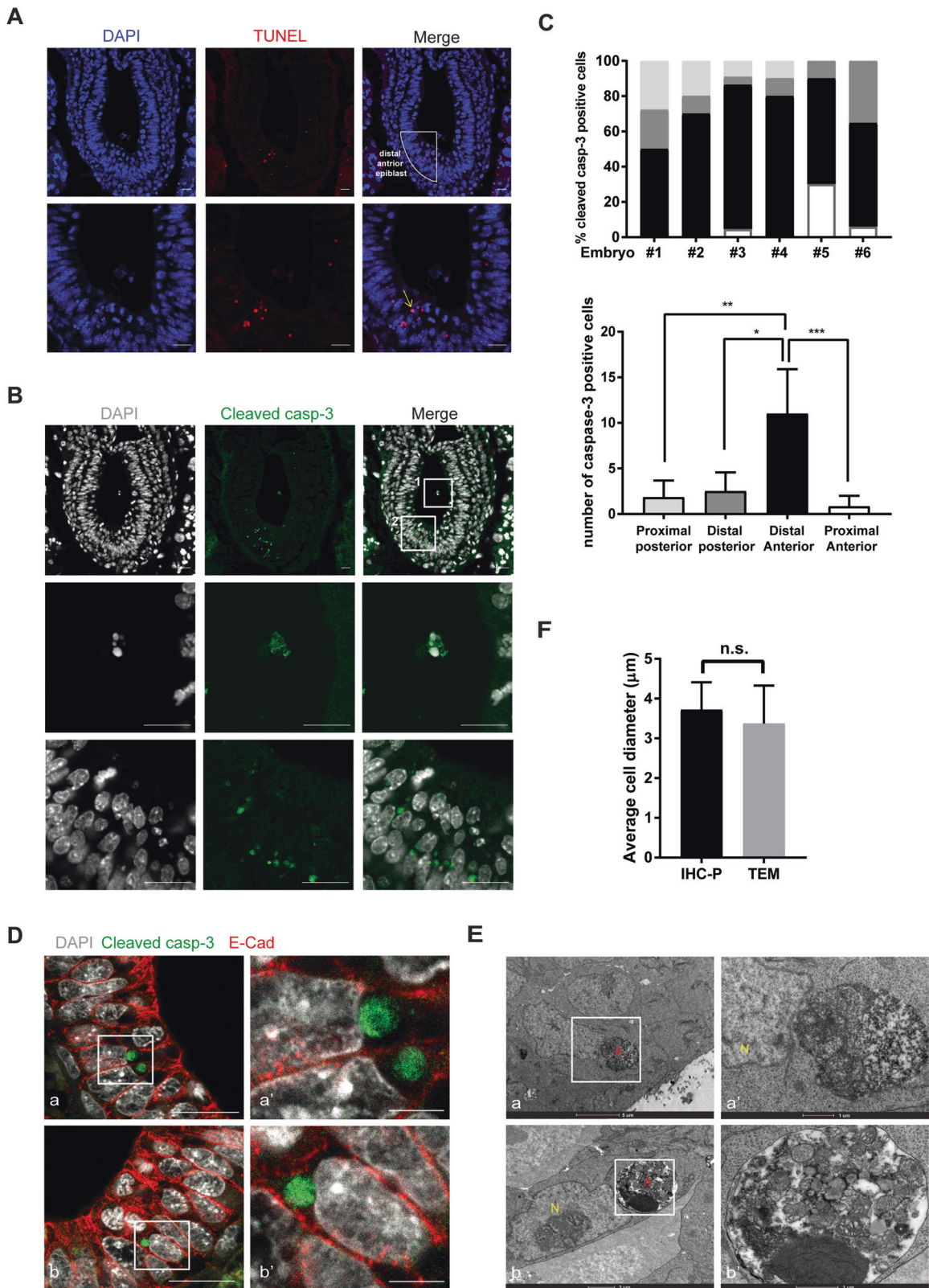
free ribosome without ER. Swollen ER containing ribosomes were found in proximity to this large vesicle, suggesting a possible fusion of the ER to the Ribo-vesicle by some physical forces, and the release of the free ribosome inside (Fig. 5Bc, d).

Altogether, these TEM images indicate that epiblast cells at the apical side of E7.5 embryos shed their cytosolic content, including condensed nuclei and other intracellular organelles, into the lumen. Loss of such critical organelles and nuclei obviously represents an irreversible, terminal stage for these cells.

#### Apaf-1 knockout mice undergo epiblast shedding in the absence of caspase activity

To determine whether the extrusion of organelles and nuclei by the apical epiblast cells is driven by caspases, the process of





epiblast shedding was examined in Apaf-1 KO mice [29], which lack the capability to form the apoptosome complex required for the activation of the initiator caspase-9. None of the examined E7.5 Apaf-1 KO embryos differed morphologically from the WT and heterozygous embryos in their overall size, cavity size, nor in

their cellular composition (Fig. 6A, S3A). As expected, WT and heterozygous embryos displayed strong cleaved caspase-3 and caspase-9 staining that co-localized with fragmented nuclei. In contrast, 14/15 and 10/10 KO embryos had no positive staining for cleaved caspase-3 or cleaved caspase-9, respectively (Fig. 6B, C).



**Fig. 2 Caspase-dependent apoptosis is activated in the post-implantation embryo at E7.5.** **A, B** IHC-P staining of E7.5 WT embryos for TUNEL (**A**, red) or cleaved caspase-3 (**B**, green). Nuclei were counterstained with DAPI (white or blue). In **A**, the distal anterior region is defined by lines and shown at higher magnification in lower panels. The yellow arrow indicates a high signal co-localizing with fragmented nuclei. In **B**, middle and lower panels are higher magnification views of boxed regions 1 (lumen) and 2 (distal anterior region) in upper panels, respectively. Scale bars, 20  $\mu\text{m}$ . **C** The number of cleaved caspase-3 positive cells was determined in different epiblast regions,  $n = 6$  embryos from 6 different litters stained in separate experiments. Data are expressed as the percent of total positive cells per region for each embryo (upper graph) and as the mean number per region (lower graph). Regions are defined by shading on the x-axis of the lower graph. Statistical significance was determined by 1-way ANOVA with Tukey's multiple comparison test,  $*p = 0.0003$ ,  $**p = 0.0001$ ,  $***p < 0.0001$ . **D** Z-stack imaging of 10  $\mu\text{m}$  IHC-P sections of E7.5 embryo stained for cleaved caspase-3 (green), E-cad (red), and nuclei (DAPI, white). **a, a'** Distal anterior region in the epiblast layer. **b, b'** Distal region in proximity to the basal side. **a', b'** High magnification views (scale bars, 5  $\mu\text{m}$ ) of boxed regions in **a, b**, respectively (scale bars, 20  $\mu\text{m}$ ). **E** TEM analysis of the E7.5 embryo epiblast. **a', b'** High magnification views of boxed regions in **a, b** respectively. **N**, nucleus of the engulfing epiblast, **A**, engulfed apoptotic body. **F** Quantitation of cell diameter of engulfed cells observed in IHC-P staining ( $n = 70$  cells from 6 embryos, originating from 6 litters) and TEM ( $n = 13$  cells from 2 embryos from the same litter). Shown are means  $\pm$  SD,  $p = 0.1269$  by two-tailed  $t$  test.

Staining of consecutive paraffin sections from the same embryo, dissected by laser capture microdissection (LMD) and genotyped by polymerase chain reaction (PCR), indicated that heterozygous embryos stained for cleaved caspase-3, caspase-9, and lamin A at identical sites corresponding to a single cell and co-localizing with nuclear fragments within that cell. These were localized within the lumen and the distal anterior region (Fig. 6D), similar to staining seen in WT Apaf-1 mice (Fig. S4B, C). In contrast, Apaf-1 KO embryos were negative for all three antibodies, in both the epiblast layer and the lumen (Fig. 6E). Interestingly, free nuclei were present in the lumen of the KO embryos, although, unlike the WT and heterozygous embryos, these nuclei were not fragmented and remained intact but condensed (Fig. 6F, Fig. S4B). Thus, caspase-3 and -9 are not activated in the KO embryos, ruling out the possibility of alternative mechanisms activating caspases in an Apaf-1-independent manner [30].

Importantly, the shedding process occurred unabated in the KO embryos; cell fragments detaching from the apical side into the lumen were detected in all genotypes, mostly from cells that lacked nuclei (Fig. 6G). The morphology of the KO embryo observed in TEM images was normal, displaying pseudostratified epiblast cells with an average size of  $8 \times 19 \mu\text{m}$ , and small enucleated epiblast cells at the apical side, with an average size of  $2.5\text{--}5 \mu\text{m}$  (Fig. 6G), similar to the WT embryos. Membrane-enclosed cytosolic fragments ( $100 \text{ nm}\text{--}3 \mu\text{m}$ ) containing different organelles were observed in the KO embryos as in WT/heterozygous embryos. Furthermore, the same type of Ribo-like vesicles and other large vesicles were observed in the lumen of the KO embryos (Fig. S4D), suggesting that this process is also Apaf-1 and caspase-independent. This, combined with the detection of shed cell fragments with condensed nuclei lacking active caspase staining described above, indicates that an Apaf-1, caspase-independent mechanism drives the extrusion of nuclear-containing cytosolic fragments.

## DISCUSSION

Here, we describe an alternative caspase-independent terminal cell state involving cell shedding and extrusion, shown here for the first time at E7.5, which continues to operate in Apaf-1 KO mice, in contrast to the canonical intrinsic apoptosis observed in E5.5–7.5 embryos. Despite the lack of caspase-dependent apoptosis, the overall morphology of E5.5–E7.5 embryos is normal in the absence of Apaf-1, suggesting that compensatory caspase-independent mechanisms replace the original function of caspase activation in the cells, as previously suggested [31]. The distinctive cell shedding process may be one such means.

The mechanism controlling cell shedding is still unknown. Once in the lumen, extruded nuclei may undergo anoikis-like apoptosis, indicated by the active caspase-3 positive immunostaining associated with fragmented nuclei surrounded by traces of cytosol, which were sometimes observed within the lumen of

WT embryos. Thus, caspases may also be activated as a mechanism to eliminate the cell-derived fragments after their extrusion. Not surprisingly, in the Apaf-1 KO embryos, all the extruded nuclei remain full-sized in the lumen with no fragmentation. The eventual fate of membrane-free organelles such as mitochondria and rough ER, which also accumulated in the lumen, remains to be determined in later stages of development when the embryo invaginates into the cavity.

The shed fragments observed in the E7.5 mouse embryo differ from previously described extracellular vesicles, such as the much smaller ectosomes ( $\sim 50 \text{ nm}\text{--}1 \mu\text{m}$  in diameter) and exosomes ( $\sim 40\text{--}160 \text{ nm}$ ), both of which function in cell-to-cell communication [32]. They also differ from cell extrusion from organized epithelial tissue, such as the mammalian small intestine and mammary gland. There, whole cells are extruded from the underlying basal lamina into the lumen as neighboring epithelial cells produce extensions pressing underneath the shed cell [33, 34]. In some cases, live cells are extruded, while in other cases, caspase-3 is activated prior to the release of the apoptotic cell into the lumen [34, 35]. In contrast, the process of shedding in the mouse embryo shown here involves a partial segmentation of the apical cells by enucleation, leaving remnants of a nucleus-free cell at the apical side. Furthermore, in the mouse embryo, shedding is caspase-independent. In both cases, however, the process preserves the continuity of the apical surface.

Other phenomena that partially share similarities with the shedding in E7.5 mouse embryos are apocrine and holocrine secretion [36, 37]. During these processes, entire portions of the cell are released, similar to the cytosolic fragments released from the apical cells in the mouse embryo. In apocrine secretion, observed in numerous metazoan polarized epithelia of secretory organs, a cell loses a portion of its cytoplasmic content by pinching off large apical protrusions but is then completely or partially renewed, differing from the shedding in the E7.5 embryo, which is a terminal process. Holocrine secretion, which occurs, for example, in the sebaceous glands, is a type of programmed cell death in which "complete secretion" occurs as the cell's entire material, including the nucleus, is released into the lumen, the cell membrane breaks down and the cell becomes completely dissolved. In this aspect, it is similar to the extrusion process in the E7.5 mouse embryo, yet in the latter, a small portion of the cell remains with an intact cell membrane. Thus, the extrusion process in the early mouse embryo is distinct from other described secretion/extrusion phenomena, although shared features may ultimately shed light on the mechanism of this atypical cell fate.

The putative role of this newly identified process can only be speculated at this stage. It is currently understood that a high mitotic rate leads to rapid embryo growth from E5.5 to E7.5, including the expansion of the cavity, which continues to maintain its round shape. As in all cellular processes, the expansion process should be balanced in some manner to prevent

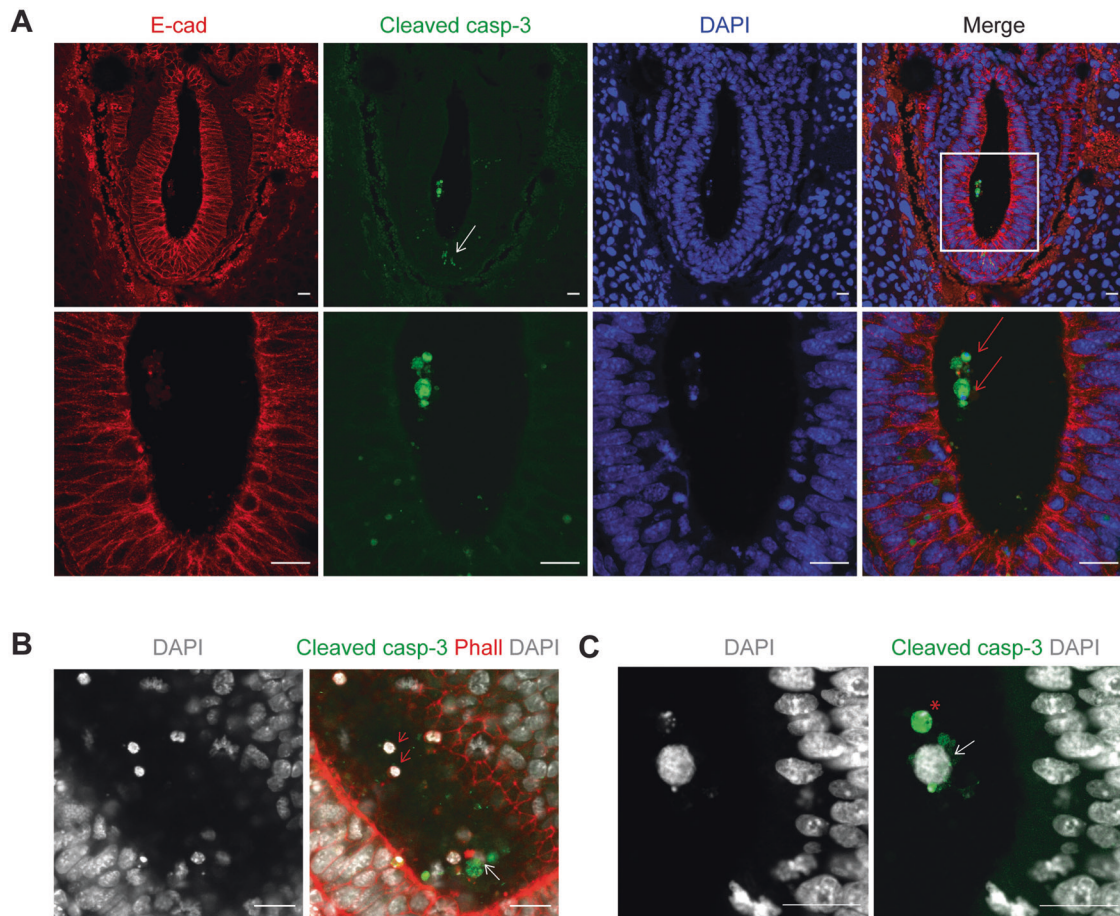


**Fig. 3 Analysis of apoptotic and condensed nuclei within the lumen of E7.5 embryos.** **A** IHC-P staining of E7.5 WT embryo for cleaved caspase-3 (green) and E-cadherin (E-cad, red), nuclei were counterstained with DAPI (blue). Lower panels are a higher magnification view of the boxed region in upper panels. Red arrows indicate a strong signal of cleaved caspase-3 co-localizing with fragmented nuclei in the lumen, and a weaker signal detected in the distal epiblast cells is marked by the white arrow. **B** Whole-mount staining of E7.5 embryo for cleaved caspase-3 (green), F-actin (phalloidin, red), and nuclei (DAPI, white). Red arrows indicate condensed nuclei without cytosol and white arrow indicates positive cleaved caspase-3 signal co-localizing with the fragmented nucleus. Shown is a representative high-resolution image, similar nuclei were observed in 20/24 embryos examined. **C** IHC-P staining of E7.5 embryo for cleaved caspase-3 (green) and nuclei (DAPI, white). A red asterisk indicates a degraded nucleus with high active caspase staining, white arrow marks a rounded, condensed nucleus with minimal caspase staining. Shown is a representative high-resolution image, similar nuclei were observed in 16/17 embryos examined. All scale bars, 20  $\mu$ m.

hyperproliferation. Cell death has been shown in many systems to be a means by which cell numbers can be limited, and based on this precedent, it is possible that the shedding serves to restrain mitosis in a sub-population of epiblasts, as the enucleated cells can no longer divide. This may function in parallel to, and as a backup for, other death pathways that limit cell numbers. It is interesting to note that in contrast to apoptosis, the shedding process leaves behind a cell remnant within the apical side of the epiblast. Whether this contributes in some manner to the sculpting of the cavity, and maintenance of its shape and symmetry, remains to be determined. In addition, the release of the majority of the cytoplasm to the lumen may contribute fluid to the lumen for further expansion, in a paralogous manner to cells undergoing division at earlier stages of development [14].

The cells undergoing enucleation and shedding have apparently lost their contact with the BM. It is possible that this detachment is a signal to trigger shedding. Interestingly, ectopic expression of N-cad in embryos at stages when E-cad normally predominates results in the shedding of groups of whole cells into the lumen, presumably as a result of changes in BMP signaling and premature EMT-like motility [38]. While this differs from the shedding observed here, which involves partial fragments of individual cells, this may offer a clue suggesting that changes in

adhesion are involved in the cell shedding. Previous reports showed that the nuclei of epiblast cells undergoing mitosis move from the basal to the apical side, in response to signals released from the BM, followed by cell detachment from the BM and completion of mitosis at the apical side [18, 39, 40]. Our data indicate that the detached shedding cells do not harbor mitotic markers, and thus are unlikely to form from mitotic cells. It is possible, however, that the shed cells arise from those that detach but fail to progress to mitosis, or are post-mitotic daughter cells that fail to re-attach to the BM.

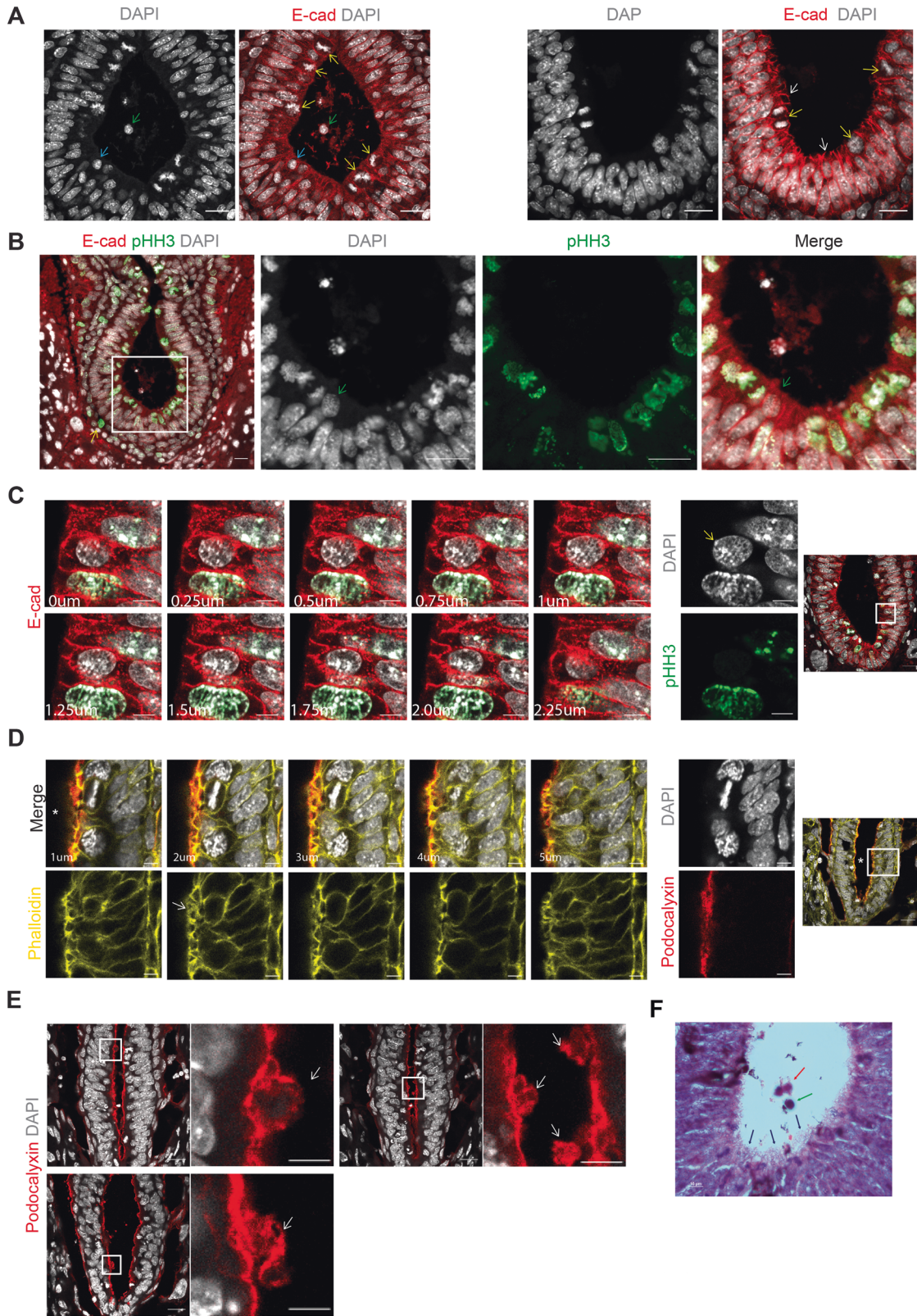
To conclude, mouse early embryonic development from the late peri-implantation stage to the end of gastrulation combines canonical apoptosis with a novel caspase-independent process of enucleation and shedding. The epiblast shedding is likely to counter-balance the accelerated growth in cell number that occurs at this post-implantation stage.

## MATERIALS AND METHODS

### Mouse models

C57BL/6J01aHsd mice were purchased from ENVIGO and maintained on a 12:12 h light–dark cycle and provided with food and water ad libitum. Eight- to 16-week-old F1 female mice were mated with F1 male mice, and





embryos were dissected at E5.5–7.5. Apaf-1 heterozygous mice, kindly provided by Tak W. Mak [29], were maintained on a C57BL/6J background and mated as above. Multiple litters were obtained; the number of embryos used for each experiment was practically determined by the number of matings and litters available, and the limitations of the assay

applied (e.g., fewer repeats for more labor-intensive TEM studies), and are indicated in the relevant figure legends. Embryos were excluded from analysis if damaged during surgery or preparation for staining. All experiments were in compliance with the Institutional Animal Care and Use Committee (IACUC) regulations (Permission# 12410419-2).



**Fig. 4 Epiblast cells at the apical side shed their content into the lumen in E7.5 embryos.** **A** IHC-P staining of E7.5 embryo for E-cadherin (E-cad, red) and nuclei (DAPI, white). Yellow arrows mark numerous cells at the apical side at different stages of mitosis, a rounded nucleus within the epiblast layer at the apical side and a free nucleus of the same size and shape in the lumen are indicated by blue and green arrows in the left panels, respectively. In right panels, apical epiblast cells lacking nuclei are marked by white arrows. Similar observations were made in more than 20 embryos examined by E-cadherin staining. **B** IHC-P staining of E7.5 embryo for pHH3 (mitotic marker, green), E-cadherin (red), and nuclei (DAPI, white). The boxed region in the left panel is shown at higher magnification in the remaining panels. Yellow arrow, cell in the visceral endoderm that stained positive for pHH3; green arrow, rounded condensed non-mitotic nucleus at the apical side. Shown is a representative image from 1 of 10 embryos examined. **C** Z-stacks of 10  $\mu\text{m}$  paraffin sections from E7.5 embryo stained for pHH3 (green), E-cadherin (red), and DAPI (white). Stacked images are from the boxed region in the low magnification image (scale bar, 5  $\mu\text{m}$ ) of the embryo shown in the right-most panel. Yellow arrow indicates one cell at the apical side with a rounded nucleus that does not stain for pHH3. See also Movies 1 and 2. **D** Z-stacks of 5  $\mu\text{m}$  frozen sections from E7.5 embryo stained for phalloidin (green), Podocalyxin (red), and DAPI (white). Stacked images are from the boxed region in the low magnification image (scale bar, 5  $\mu\text{m}$ ) of the embryo shown in the right-most panel. \*, lumen. Arrow points to a cluster of 3 enucleated apical cells; see also Movie 3, which focuses on these cells. **E** Staining of a frozen section from E7.5 embryo for Podocalyxin (red) and DAPI (white). The right panel is a higher magnification view of the boxed region in the left panel, for each pair of images. Arrows indicate extrusion of the apical membrane into the lumen. All scale bars are 20  $\mu\text{m}$  unless otherwise indicated. Similar structures were seen in all 5 embryos stained for Podocalyxin. **F** Paraffin section of E7.5 embryo stained with H&E to delineate cytoplasm and nuclei. Black arrows, small enucleated cell remnants at the apical surface; green arrow, shed free nucleus within the lumen; red arrow, shed nucleus surrounded by trace cytoplasm within the lumen. Shown is a representative image from one of three embryos analyzed. Scale bar, 10  $\mu\text{m}$ .

### Antibodies

Primary antibodies used for immunostaining are as follows: cleaved caspase-3, Cell Signaling, cat# 9664; cleaved caspase-9, MyBioSource, cat# MBS852276; E-cadherin, Cell Signaling, cat# 14472; OCT4, Santa Cruz, cat# sc-5279; Phospho histone H3, Abcam cat# ab5176; LC3B, Cell Signaling, cat# 2775; cleaved lamin A, Cell Signaling, cat# 2035; Podocalyxin, R&D Systems, cat# MAB1556. Secondary antibodies used were either Alexa Fluor 488 conjugated goat anti-rabbit IgG, or Alexa Fluor 555 conjugated goat anti-mouse IgG or anti-rat IgG (Invitrogen, cat# A11034, A21424, A21434, respectively).

### IHC staining of paraffin sections (IHC-P)

For immunohistological analysis, embryos at E5.5 and E7.5 were isolated together with their decidua from the uterus of pregnant mice. The embryos and decidua were fixed in 4% paraformaldehyde and embedded in paraffin following standard protocols. Sagittal sections of 6 mm were processed for IHC. De-waxing was performed in xylene, followed by hydration in graded alcohols. Antigen retrieval was carried out in sodium citrate buffer, pH 6.0 to enhance staining. Permeabilization in PBT (0.1% Triton-X 100 in PBS) was performed for 10 min and sections were then incubated with 5% NGS + 0.5% BSA in PBS-T (0.02% Tween20 in PBS), followed by overnight incubation with primary antibody diluted in Blocking Solution and then secondary antibodies. Finally, nuclei were counterstained with DAPI. For TUNEL staining, deparaffinized and rehydrated sagittal sections were stained using the Apoptag commercial kit (Sigma-Aldrich, cat# S7165) according to the manufacturer's instructions. Briefly, after incubation with 20  $\mu\text{g}/\text{mL}$  proteinase K, samples were incubated in TdT-enzyme solution followed by anti-digoxigenin conjugate and finally stained with DAPI. For H&E staining, deparaffinized and rehydrated sections were stained with hematoxylin and eosin according to standard histology protocols. All slides were mounted with Immu-Mount (Bar-Naor, cat# 9990402). Images were acquired using Zeiss LSM780, Zeiss LSM800 or Zeiss LSM900 confocal Axio Observer Z1 inverted microscopes equipped with 20 $\times$  Plan-Apochromat objective, N.A. 0.8, 40 $\times$  C-Apochromat water-immersion objective, N.A. 1.2, and 100 $\times$  EC Plan-Neofluar oil-immersion objective, N.A.1.3. Images were processed using ZEN software (version 2.4).

### Whole-mount staining and sample lysis

E5.5 to E7.5 embryos isolated from the uterus were fixed with 4% paraformaldehyde overnight, followed by washing with PBS. Tissue permeabilization was carried out for 15 min in 0.1 M Glycine, 0.3% Triton X-100/PBS. The embryos were incubated overnight in primary antibody diluted in 10% NGS/PBT followed by secondary antibodies with Phalloidin (Sigma-Aldrich, cat# 65906). Embryos were stained with DAPI and mounted in PBS in iBidi plates. Images were acquired using a Zeiss LSM 780 or 800 confocal scanning systems, as detailed above. Immediately after imaging, Apaf-1 embryos were individually collected and lysed in 10  $\mu\text{L}$  lysis buffer (50 mM KCl, 1.5 mM  $\text{MgCl}_2$ , 10 mM Tris-Cl pH 8.0, 0.5% NP-40, 0.5% Tween-20, 100  $\mu\text{g}/\text{mL}$  proteinase K) at 56  $^\circ\text{C}$  for 4 h, briefly centrifuged, incubated for 10 min at 95  $^\circ\text{C}$  to inactivate proteinase K, and centrifuged again. Each

cell lysate was subsequently analyzed by PCR for genotyping analysis as described.

### IHC staining of frozen sections

For immunohistological analysis, E7.5 embryos were isolated together with their decidua from the uterus of pregnant mice. The embryos and decidua were fixed in 4% paraformaldehyde overnight at 4  $^\circ\text{C}$  and then washed with PBS. Samples were incubated for 8 h with 15% sucrose (AnalaR NORMAPUR analytical reagent, cat# 57-50-1) in PBS, and 30% sucrose overnight at 4  $^\circ\text{C}$ . Samples were passed through graded 30% sucrose:OCT (Tissue-Tek, 4583) combinations (2:1 1:1, 1:2 each for 30 min) and finally to 100% OCT twice for 45 min. Samples were placed in a mold with OCT on dry ice until frozen. Sagittal sections of 12 mm were cut using a cryostat microtome and processed for IHC. Slides were incubated at 56  $^\circ\text{C}$  for 1 h, washed in PBS for 10 min, borders were determined by the liquid blocker PAP-PEN followed by permeabilization in PBT (0.1% Triton-X 100 in PBS) for 10 min. Sections were then incubated with blocking buffer (5% NGS + 0.5% BSA in PBS-T (0.02% Tween20 in PBS)) for 1 h in a humidity chamber, followed by overnight incubation with primary antibody diluted in Blocking Solution. Sections were washed 3 times with PBS-T for 10 min, and secondary antibodies together with Phalloidin diluted in Blocking Solution were applied for 1.5 h at room temperature. Sections were washed 3 times with PBS-T for 10 min. Finally, nuclei were counterstained with DAPI (diluted in PBS). All slides were mounted and images were acquired by confocal microscopy as detailed above.

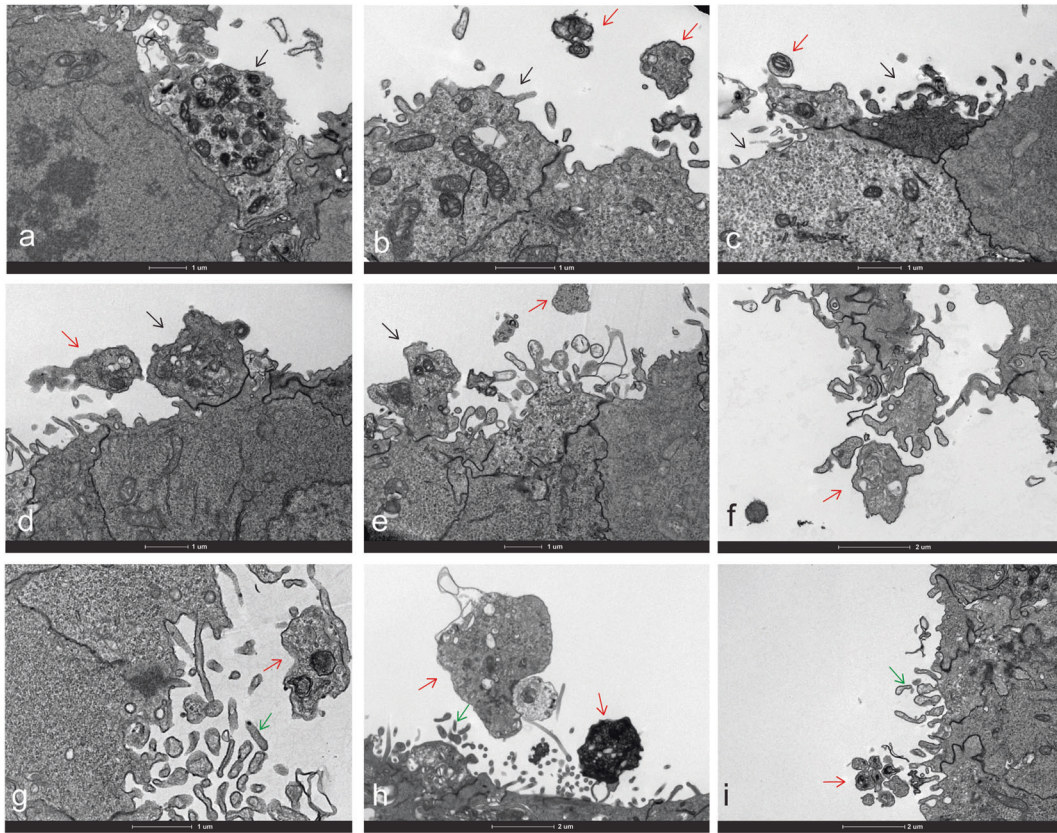
### LMD and sample lysis

Prior to LMD, all membrane slides (415190-9041-000 PALM Systems) were deparaffinized in xylene and rehydrated through graded ethanol washes, and stained with hematoxylin and eosin. After a minimum of 24 h air-drying, LMD was performed (PALM Laser microdissection microscope, Zeiss) to isolate the E7.5 embryos from the maternal tissue. Tissue was collected into AdhesiveCaps (415190-9181-000 PALM Systems) and stored at 4  $^\circ\text{C}$  until DNA extraction. Collected samples were individually lysed in 10  $\mu\text{L}$  lysis buffer (50 mM KCl, 1.5 mM  $\text{MgCl}_2$ , 10 mM Tris-Cl pH 8.0, 0.5% NP-40, 0.5% Tween-20, 100  $\mu\text{g}/\text{mL}$  proteinase K) at 56  $^\circ\text{C}$  for 4 h. Each cell lysate was subsequently analyzed by PCR for genotyping.

### Genotyping by PCR analysis

To determine the genotype of Apaf-1 mice/embryos, genomic DNA was isolated from tail clippings, E7.5 embryos, or LMD. DNA was amplified by PCR using forward primers 5'-CTCAAACACCTCCTCCACAA-3' for WT sequence, and 5'-GGGCCAGCTCATTCTC-3' for mutant sequence, and reverse primer 5'-GTCATCTGGAAGGG CAGCGA-3' to amplify a fragment of 800 bp for the Apaf-1 WT allele and 600 bp for the Apaf-1 KO allele. All genotyping was performed after immunostaining and imaging, so the investigator was blinded as to Apaf-1 status during the analysis of staining results.

A



B

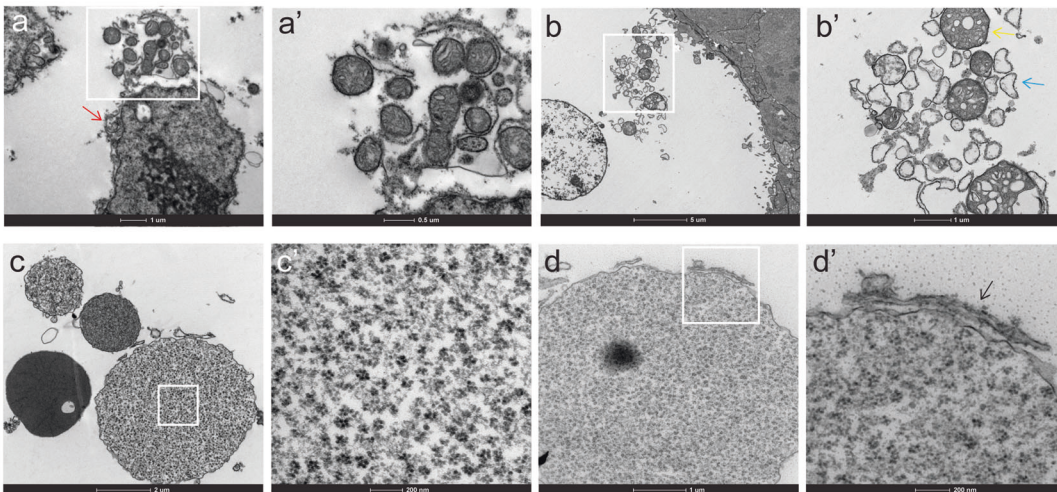


**Fig. 5 TEM of E7.5 mouse embryos showing apical shedding. A** Images of epiblast cells at the apical side shedding cytosolic fragments into the lumen. a, b Small apical cells without nuclei and with many mitochondria, marked by the black arrow. Red arrows, detached fragments surrounded by membrane in the lumen. c Shedding in progress. The red arrow indicates a mitochondrion inside an extruded vesicle at the apical side, black arrows, two small nucleated cells at the apical side. d, e Red and black arrows indicate detached cell fragments and small cells connected to the epiblast layer, respectively. f Red arrow, large cytosolic fragments released into the lumen. g–i Comparison of the shed cytosolic fragment containing organelles (red arrows) to microvilli (green arrow) at different magnifications. Shown are representative images from eight embryos examined. **B** Images of cytosolic content undergoing degradation in the lumen, including free mitochondria and ER without any surrounding membrane (a, a', b, b'), yellow arrow, swollen mitochondrion, blue arrow, swollen ER. The red arrow in (a) indicates a floating nucleus surrounded by cytoplasm. c, c', d, d' large, rounded vesicles of different densities and content, including ribo-vesicles containing free ribosomes without ER. In d', black arrow marks rough ER in proximity with the surface of a ribo-vesicle, possibly undergoing fusion. Panels at the right marked by (') are high magnification images of the respective panels at the left.



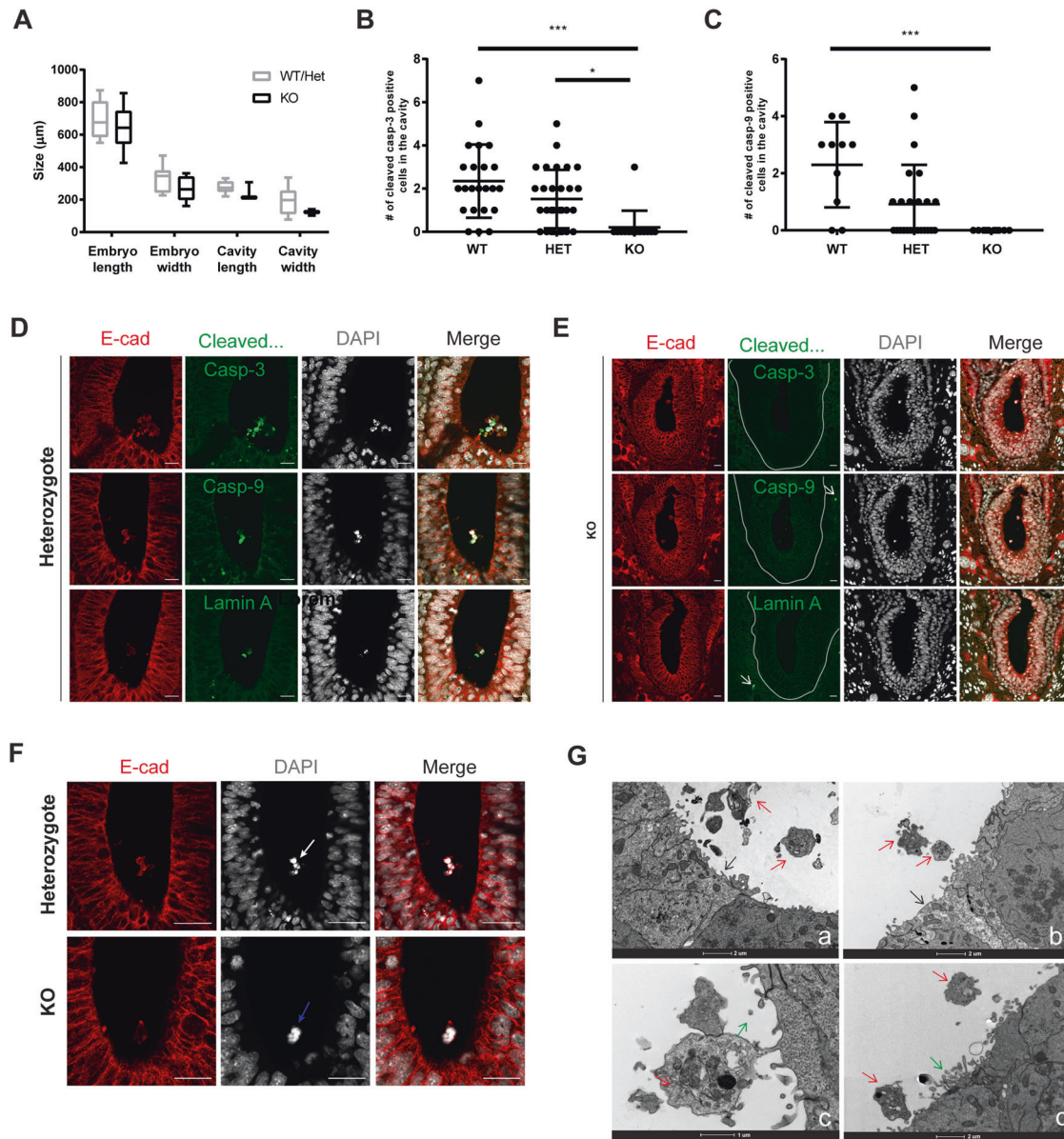


**Fig. 6 Apaf-1 KO embryos lack caspase activation and nuclear fragmentation.** **A** Measurement of embryo and cavity size of E7.5 embryos derived from Apaf-1 heterozygous intercrosses. Shown is mean  $\pm$  SD,  $n = 11$  WT/Het and  $n = 6$  KO embryos from 3 litters. Two-tailed  $t$  tests indicated no statistical significance ( $p > 0.05$ ) between pairs for each parameter examined. **B** Quantitation of cleaved caspase-3 positive cells, detected by whole-mount staining, in the cavity of E7.5 embryos derived from Apaf-1 heterozygous intercrosses. Shown is mean  $\pm$  SD (WT,  $n = 23$ , Het,  $n = 30$ , KO,  $n = 15$  embryos from 9 litters). Statistical significance was determined by one-way ANOVA with Tukey's multiple comparisons test, \*\*\* $p < 0.0001$ , \* $p = 0.0109$ . **C** Quantitation of cleaved caspase-9 positive cells, as in **(B)**. WT,  $n = 10$ , Het,  $n = 24$ , KO,  $n = 10$  embryos from 6 litters. Statistical significance was determined by one-way ANOVA with Tukey's multiple comparisons test, \*\* $p = 0.0005$ . **D, E** IHC-P staining of serial sections of an E7.5 heterozygous **(D)** or KO **(E)** embryo for cleaved caspase-3, cleaved caspase-9, or cleaved lamin A (green) with E-cadherin (E-cad, red) and DAPI (white). The white line in **E** delineates the boundaries of the embryo, white arrows indicate positive caspase-3 staining in the heterozygous maternal uterine tissue. Shown are representative images from one of  $n = 5$  Het and  $n = 2$  KO embryos. **F** IHC-P staining of E7.5 heterozygote and KO embryos for E-cadherin (red), nuclei (DAPI, white) as in **(D, E)**. White arrow, fragmented nucleus, blue arrow, condensed nucleus. Scale bars in **D–F**: 20  $\mu$ m. **G** TEM of Apaf-1 KO embryos at E7.5 showing shedding and absence of nuclei at the apical side. Black arrows (a, b) indicate enucleated cells at the apical region that shed cytosolic fragments into the lumen (red arrows). In c, d, large cytosolic fragments (red arrows) contrast with small microvilli (green arrows). Shown are representative images from 1 of 5 KO embryos examined.

#### Transmission electron microscopy

E7.5 embryos were fixed in 3% paraformaldehyde, 2% glutaraldehyde in 0.1 M cacodylate buffer containing 5 mM  $\text{CaCl}_2$  (pH 7.4), then post-fixed in 1% osmium tetroxide supplemented with 0.5% potassium hexacyanoferrate trihydrate and potassium dichromate in 0.1 M cacodylate, stained with 2% uranyl acetate, dehydrated in graded ethanol solutions and embedded in Agar 100 epoxy resin (Agar Scientific Ltd., Stansted, UK). Ultrathin transverse sections (70–90 nm) were viewed and photographed with an FEI

Tecni SPIRIT (FEI, Eindhoven, Netherlands) transmission electron microscope operated at 120 kV and equipped with an EAGLE CCD Camera.

#### FIB-SEM volume imaging

Samples for FIB-SEM volume imaging were prepared as for TEM. Data were acquired using a Helios-600 Dual Beam (Thermo Fisher Scientific, USA). SEM images were recorded at 2.2 kV with 340 pA, in the immersion lens



mode. X–Y pixel size was 6.4 nm. For serial slices milling an ion beam current of 0.46 nA at 30 kV was used with a step size of 10 nm.

### Sample size, sample collection, and experiment metrics

Experiments were repeated in multiple embryos from different mouse litters as detailed in the figure legends for each specific experiment. When indicated, different sections from the same embryo were examined. For analysis of Apaf-1 mice, the number of embryos of each genotype assayed is indicated in the figure legends.

### Quantification and statistical analysis

Statistical analysis, i.e., two-tailed *t* test for comparisons between pairs of samples or one-way ANOVA for comparisons among multiple samples, was performed using GraphPad Prism 7.05 software with  $p \leq 0.05$  considered significant. Details of specific tests, *n*, and appropriate parameters are provided in relevant figure legends. *F*-tests were performed to estimate variance within each sample and to confirm equal variance of samples; where appropriate, D'Agostino & Pearson normality tests were used to confirm the normal distribution of the population.

### DATA AVAILABILITY

Data sharing is not applicable to this article as no datasets were generated or analyzed during the current study.

### REFERENCES

- Zakeri Z, Penalzoza CG, Smith K, Ye Y, Lockshin RA. What cell death does in development. *Int J Devel Biol.* 2015;59:11–22.
- Hernández-Martínez R, Covarrubias L. Interdigital cell death function and regulation: new insights on an old programmed cell death model. *Dev Growth Differ.* 2011;53:245–58.
- Suzanne M, Steller H. Shaping organisms with apoptosis. *Cell Death Diff.* 2013;20:669–75.
- Manjón C, Sánchez-Herrero E, Suzanne M. Sharp boundaries of dpp signalling trigger local cell death required for drosophila leg morphogenesis. *Nat Cell Biol.* 2007;9:57–63.
- Kuan C-Y, Roth KA, Flavell RA, Rakic P. Mechanisms of programmed cell death in the developing brain. *Trends Neurosci.* 2000;23:291–7.
- Brison DR, Schultz RM. Apoptosis during mouse blastocyst formation: evidence for a role for survival factors including transforming growth factor  $\alpha$ . *Biol Reprod.* 1997;56:1088–96.
- El-Shershaby A, Hinchliffe J. Cell redundancy in the zona-intact preimplantation mouse blastocyst: a light and electron microscope study of dead cells and their fate. *Development.* 1974;31:643–54.
- Morris SA, Teo RT, Li H, Robson P, Glover DM, Zernicka-Goetz M. Origin and formation of the first two distinct cell types of the inner cell mass in the mouse embryo. *Proc Natl Acad Sci USA.* 2010;107:6364–9.
- Byrne A, Southgate J, Brison D, Leese H. Analysis of apoptosis in the pre-implantation bovine embryo using tunel. *Reproduction.* 1999;117:97–105.
- Coucounavis E, Martin GR. Signals for death and survival: a two-step mechanism for cavitation in the vertebrate embryo. *Cell.* 1995;83:279–87.
- Coucounavis E, Martin GR. Bmp signaling plays a role in visceral endoderm differentiation and cavitation in the early mouse embryo. *Development.* 1999;126:535–46.
- Abud HE. Shaping developing tissues by apoptosis. *Cell Death Differ.* 2004;11:797.
- Bedzhov I, Zernicka-Goetz M. Self-organizing properties of mouse pluripotent cells initiate morphogenesis upon implantation. *Cell.* 2014;156:1032–44.
- Kim YS, Fan R, Kremer L, Kuempel-Rink N, Mildner K, Zeuschner D, et al. Deciphering epiblast lumenogenesis reveals proamniotic cavity control of embryo growth and patterning. *Sci Adv.* 2021;7:eabe1640.
- Singla S, Iwamoto-Stohl LK, Zhu M, Zernicka-Goetz M. Autophagy-mediated apoptosis eliminates aneuploid cells in a mouse model of chromosome mosaicism. *Nat Commun.* 2020;11:1–15.
- Molé MA, Weberling A, Fässler R, Campbell A, Fishel S, Zernicka-Goetz M. Integrin  $\beta 1$  coordinates survival and morphogenesis of the embryonic lineage upon implantation and pluripotency transition. *Cell Rep.* 2021;34:108834.
- Snow MH. Cell death in embryonic development. Perspectives on mammalian cell death. Oxford University Press, Oxford; 1987. p. 202–28.
- Gardner R, Cockroft D. Complete dissipation of coherent clonal growth occurs before gastrulation in mouse epiblast. *Development.* 1998;125:2397–402.
- O'Farrell PH, Stumpff J, Su TT. Embryonic cleavage cycles: how is a mouse like a fly? *Curr Biol.* 2004;14:R35–R45.
- Streffler C, Beuning DV, Molls M, Zamboglou N, Schulz S. Kinetics of cell proliferation in the pre-implanted mouse embryo in vivo and in vitro. *Cell Prolif.* 1980;13:135–43.
- Poelmann R. Differential mitosis and degeneration patterns in relation to the alterations in the shape of the embryonic ectoderm of early post-implantation mouse embryos. *Development.* 1980;55:33–51.
- Pereira PN, Dobreva MP, Graham L, Huylebroeck D, Lawson KA, Zwijsen A. Amnion formation in the mouse embryo: the single amniochorionic fold model. *BMC Dev Biol.* 2011;11:48.
- Tam P, Beddington R. Establishment and organization of germ layers in the gastrulating mouse embryo. In: Derek J Chadwick JM, editor. Postimplantation development in the mouse: Ciba foundation symposium 165. Wiley: Chichester; 1992. p. 27–49.
- Manova K, Tomihara-Newberger C, Wang S, Godelman A, Kalantry S, Witty-Blease K, et al. Apoptosis in mouse embryos: elevated levels in pregastrulae and in the distal anterior region of gastrulae of normal and mutant mice. *Dev Dyn.* 1998;213:293–308.
- Sanders E, Torkkeli P, French A. Patterns of cell death during gastrulation in chick and mouse embryos. *Anat Embryol.* 1997;195:147–54.
- Los M, Wesselborg S, Schulze-Osthoff K. The role of caspases in development, immunity, and apoptotic signal transduction: lessons from knockout mice. *Immunity.* 1999;10:629–39.
- Lee SC, Chan J, Clement MV, Pervaiz S. Functional proteomics of resveratrol-induced colon cancer cell apoptosis: caspase-6-mediated cleavage of lamin A is a major signaling loop. *Proteomics.* 2006;6:2386–94.
- Menon V, Ghaffari S. Erythroid enucleation: a gateway into a “bloody” world. *Exp Hematol.* 2021;95:13–22.
- Yoshida H, Kong Y-Y, Yoshida R, Elia AJ, Hakem A, Hakem R, et al. Apaf1 is required for mitochondrial pathways of apoptosis and brain development. *Cell.* 1998;94:739–50.
- Nagasaka A, Kawane K, Yoshida H, Nagata S. Apaf-1-independent programmed cell death in mouse development. *Cell Death Diff.* 2010;17:931–41.
- Yuan J, Kroemer G. Alternative cell death mechanisms in development and beyond. *Genes Dev.* 2010;24:2592–602.
- Cocucci E, Meldolesi J. Ectosomes and exosomes: shedding the confusion between extracellular vesicles. *Trends Cell Biol.* 2015;25:364–72.
- Williams J, Duckworth C, Burkitt M, Watson A, Campbell B, Pritchard D. Epithelial cell shedding and barrier function: a matter of life and death at the small intestinal villus tip. *Vet Pathol.* 2015;52:445–55.
- Bullen TF, Forrest S, Campbell F, Dodson AR, Hershman MJ, Pritchard DM, et al. Characterization of epithelial cell shedding from human small intestine. *Lab Invest.* 2006;86:1052.
- Gudipaty SA, Rosenblatt J. Epithelial cell extrusion: pathways and pathologies. *Semin Cell Dev Biol.* 2017;67:132–40.
- Farkaš R. The complex secretions of the salivary glands of drosophila melanogaster, a model system. In: Cohen E. MB, (ed). Extracellular composite matrices in arthropods. Cham: Springer; 2016. p. 557–600.
- Farkaš R, Ďátková Z, Mentelova L, Löw P, Beňová-Liszeková D, Beňo M, et al. Apocrine secretion in drosophila salivary glands: Subcellular origin, dynamics, and identification of secretory proteins. *PLoS ONE.* 2014;9:e94383.
- Basilicata MF, Frank M, Solter D, Brabletz T, Stemmler MP. Inappropriate cadherin switching in the mouse epiblast compromises proper signaling between the epiblast and the extraembryonic ectoderm during gastrulation. *Sci Rep.* 2016;6:1–15.
- Mathiah N, Despin-Guitard E, Stower M, Nahaboo W, Eski ES, Singh SP, et al. Asymmetry in the frequency and position of mitosis in the mouse embryo epiblast at gastrulation. *EMBO Rep.* 2020;21:e50944.
- Ichikawa T, Nakazato K, Keller PJ, Kajiura-Kobayashi H, Stelzer EH, Mochizuki A, et al. Live imaging of whole mouse embryos during gastrulation: migration analyses of epiblast and mesodermal cells. *PLoS ONE.* 2013;8:e64506.

### ACKNOWLEDGEMENTS

We thank the Stem Cells and Advanced Cell Technologies Unit at the Weizmann Institute for LMD equipment and guidance. We thank Katya Rehav (Department of Chemical Research Support, Weizmann Institute) for her expertise in performing the FIB-SEM volume imaging. We thank Dr. Yonatan Stelzer (Department of Molecular and Cellular Biology, Weizmann Institute) for reading the paper and consultations. We thank Prof. Tak Wah Mak (University of Toronto) for providing the Apaf-1 mice. We thank Prof. Yaqub (Jacob) Hanna and Alejandro Aguilera Castrejon for consulting and assistance. This work was supported by grants from the Israel Science Foundation, Grant No. 679/

17, and from the European Research Council under the European Union's Seventh Framework Program (FP7/2007-2013/ERC grant agreement 322709) to A.K.

#### **AUTHOR CONTRIBUTIONS**

R.H. and A.K. conceived and designed the overall project; R.H. performed the experiments; S.L.-Z. performed and analyzed the EM studies; R.H. and A.K. interpreted the results; R.H., V.L.-S., S.B., and A.K. wrote and edited the paper; R.H. and S.B. generated figures and graphs; A.K. supervised the work and acquired funding for the project. All authors critically reviewed and revised the paper and approved the final paper.

#### **COMPETING INTERESTS**

The authors declare no competing interests.

#### **ETHICS STATEMENT**

Animal studies were conducted in compliance with the Institutional Animal Care and Use Committee (IACUC) regulations (Permission# 12410419-2).

#### **ADDITIONAL INFORMATION**

**Supplementary information** The online version contains supplementary material available at <https://doi.org/10.1038/s41418-021-00918-5>.

**Correspondence** and requests for materials should be addressed to Adi Kimchi.

**Reprints and permission information** is available at <http://www.nature.com/reprints>

**Publisher's note** Springer Nature remains neutral with regard to jurisdictional claims in published maps and institutional affiliations.